AGU PUBLICATIONS

JGR

Journal of Geophysical Research: Atmospheres

RESEARCH ARTICLE
10.1002/2014JD022690

**Key Points:**
- Sensitivity of convective morphology to environment is assessed
- A subset of environmental characteristics is especially influential
- Aerosol invigoration could lower anvil base height

**Correspondence to:**
M. R. Igel,
migel@rsmas.miami.edu

**Citation:**
Igel, M. R., and S. C. van den Heever (2015), The relative influence of environmental characteristics on tropical deep convective morphology as observed by CloudSat, *J. Geophys. Res. Atmos.*, *120*, 4304–4322, doi:10.1002/2014JD022690.

Received 8 OCT 2014
Accepted 18 APR 2015
Accepted article online 23 APR 2015
Published online 14 MAY 2015

©2015. American Geophysical Union. All Rights Reserved.

# The relative influence of environmental characteristics on tropical deep convective morphology as observed by CloudSat

**Matthew R. Igel[1] and Susan C. van den Heever[1]**

[1]Department of Atmospheric Science, Colorado State University, Fort Collins, Colorado, USA

**Abstract** Utilizing a previously developed CloudSat cloud object database, the sensitivity of oceanic, mature, deep convective cloud morphology to cloud-scale environmental characteristics is examined. Convective available potential energy (CAPE), aerosol optical depth, midlevel vertical velocity, and tropospheric deep shear are all used to characterize the environment. The sensitivity of various aspects of convective morphology to each one of these environmental quantities is assessed individually. The results demonstrate that clouds tend to be invigorated by higher CAPE, aerosol, and upward midlevel vertical velocity. Stronger shear tends to make clouds wider but also shallower. The relative importance of each of these and some additional environmental measures to trends in cloud morphology are compared. It is found that aerosol, deep-layer shear, and sea surface temperature tend to be the most influential environmental factors to convective morphology. The results are shown to be insensitive to the manner in which the environmental characteristics are defined. The potentially surprising weak sensitivity of cloud morphology to CAPE is discussed in detail.

## 1. Introduction and Background

Deep, moist convection occurs within many meteorological environments over the open tropical oceans. This convection is responsible for the vast majority of rainfall in these regions [*Nesbitt et al.*, 2000; *Nesbitt and Zipser*, 2003] and forms one of the primary interfaces between the tropical atmosphere and global climate [*Stephens*, 2005; *Schneider et al.*, 2010]. Because of the importance of deep convective clouds, it is crucial to understand their sensitivity to their local environmental characteristics. Some previous work has focused on the sensitivity of the ensemble effects of clouds such as precipitation or cloud fraction to local meteorological environment in the tropical, oceanic atmosphere [*Saxen and Rutledge*, 2000], while several others have pursued quantifying the sensitivity of composite cloud morphology to such variables [*Masunaga et al.*, 2005; *Riley et al.*, 2011]. In this paper, we focus on examining the sensitivity of the morphology of individual clouds to various local environmental characteristics. We use the phrase "morphology" to mean the shape of clouds as defined by various physical length scales (listed and defined in section 2.1).

The question may be asked as to why such properties of clouds matter? The size and shape of clouds influence the resultant effects of clouds on the immediate atmospheric state. For example, a cloud with a higher, and hence colder, cloud top emits less radiation to space than does a lower cloud which results in a locally enhanced warming of the column. Examining cloud size and shape may also provide insight into the inner workings of deep convective clouds [e.g., *Nesbitt et al.*, 2006; *Liu and Zipser*, 2013; *Igel*, 2014]. Determining simple relationships between clouds' morphology, local meteorological environment, and the physics that govern them are crucial to improving parameterization methods of deep convection for use in weather and climate models. Much of what is known about the size and shape of deep convection below anvil top has been derived from ground-based radar data gathered during a number of seminal field studies [*Houze Jr. and Cheng*, 1977; *Brown and Zhang*, 1997; *DeMott and Rutledge*, 1998a, 1998b; *Johnson et al.*, 1999; *Del Genio and Kovari*, 2002]. These campaigns often allowed for the collocation of sounding data in order to characterize the environment of the radar-derived morphology data. However, while thorough and in-depth investigations have been performed using these data sets, such field studies are limited in their spatial and temporal coverage.

The exact morphology of any individual deep convective cloud is a function of multiple variables. Many of these are external to the cloud, such as convective available potential energy or shear. This study examines the impacts of such external variables. Because the potential parameter space of external influences on

convection extends to many dimensions, several previously postulated direct environmental influences on convection are examined here. These are

1. *Convective available potential energy* (CAPE). CAPE is often used as the primary driver of convection in parameterization schemes of convection [*Arakawa*, 2004; *Yano and Plant*, 2012]. The reason for its frequent use is that it links the energy cycle of the atmosphere with convection in a very direct manner. When calculated to include the effects of freezing, CAPE represents a potential upper limit on the column-integrated buoyancy a moist-convecting column could realize. Therefore, it can be argued that more CAPE might yield deeper and wider clouds. The problem with this interpretation becomes that while CAPE represents the upper limit to buoyancy generation, no physical process actually requires convection to reach this limit at time scales similar to individual convective lifetimes. In the moist tropics, CAPE is often the result of small differences between the temperature and moist adiabatic profiles which yields a "skinny" profile [*Lucas et al*., 1994; *Cetrone and Houze*, 2006] due to the moist atmosphere. As a consequence, energy release tends to be slow and steady as convection develops, and a cloud is susceptible to having its growth stunted by various processes such as entrainment of drier air.
2. *Shear*. The term "shear" is used throughout this paper to mean the vertical shear of the horizontal wind. Shear has been shown to affect the dynamical flow structures around and within deep convection [*Rotunno et al*., 1988; *LeMone et al*., 1998; *Weisman and Rotunno*, 2004; *Coniglio et al*., 2006]. Different magnitudes of shear can result in different storm types and orientations [*Barnes and Sieckman*, 1984; *Johnson et al*., 2005; *Cetrone and Houze*, 2006]. One of the consequential results of the Tropical Ocean–Global Atmosphere Coupled Ocean-Atmosphere Response Experiment field campaign conducted in the early 1990s was the attribution of storm morphology to shear, including the fact that more highly sheared clouds are often observed to have wider anvils as the anvil is advected away from the main convective region [*Hildebrand*, 1998; *Halverson et al*., 1999; *Saxen and Rutledge*, 2000; *Rickenbach et al*., 2008; *Li and Schumacher*, 2011].
3. *Midlevel vertical velocity* ($\omega$500). The $\omega$500 is indicative of several physical processes potentially influential to convection [*Bony et al*., 1997; *Peters et al*., 2013; *Kumar et al*., 2014]. First, through continuity arguments, $\omega$500 can be taken to imply the magnitude and sign of surface convergence. Surface convergence can act as a direct dynamic trigger for convection; it can also act as a potential convective trigger through locally increasing low-level moisture. Second, $\omega$500 is broadly diagnostic of the convective state. A negative $\omega$500 potentially indicates the existence of convection, with more negative $\omega$500 suggestive of the existence of stronger convection and/or of broader spatial coverage of updrafts.
4. *Aerosol concentration* (AOD, as aerosol optical depth will act as a proxy for number concentration [*Andreae*, 2009]). Aerosol amount is often assumed to impact convection through its influence on the total latent heat release of deep convection storms [*Andreae et al*., 2004; *Khain et al*., 2005; *van den Heever et al*., 2006; *van den Heever and Cotton*, 2007; *Rosenfeld et al*., 2008; *Koren et al*., 2010a; *Storer and van den Heever*, 2013]. Through a process commonly referred to as "aerosol-induced convective invigoration," high-number concentrations of aerosol may delay warm rain processes thus allowing more liquid water to be lofted and freeze. This increase in freezing results in more in-cloud net latent heat release, enhanced buoyant forcing, and higher updraft velocities. Higher vertical velocities might then result in higher cloud tops and/or more anvil detrainment. For a comprehensive review of aerosol effects on deep convective clouds, see *Tao et al*. [2012].

There is also interesting evidence for complicated simultaneous regulation of clouds between these environmental characteristics, (1)–(4) [e.g., *Fan et al*., 2009; *Niu and Li*, 2012; *Storer et al*., 2014]. Because of the particular analysis method used here, several other potential influences on convective morphology are also examined and compared to factors (1)–(4) in an effort to be more exhaustive in this analysis. These include geographic location and sea surface temperature.

The influences of these environmental parameters on convection are examined below through the analysis of trends in convective length scales. Analysis as simple as quantifying anvil widths and cloud top heights has been the goal of a series of recent works and has resulted in insights into the inner workings of convection [*Igel et al*., 2014; *Igel*, 2014]. In these two prior studies, simple diagnostic length scales were used to examine the anvil-sea surface temperature (SST) feedback [*Igel et al*., 2014] and the dynamic links between convective pedestals and anvils [*Igel*, 2014]. Finally, it should be noted that the data set developed by *Igel et al*. [2014] has a very strict applicability to mature, deep convection over tropical oceans although a very general

applicability among these clouds. This strict applicability results from the highly selective identification of clouds imposed when developing this data set [*Igel et al*., 2014] which benefits the discussion. It allows us to examine a very specific subset of clouds important to the properties of the marine tropical atmosphere in a way never before possible.

This paper is organized as follows: A discussion of the broad observational framework under which this study is conducted and the other tools used are included next. In the first part of the analysis, cloud morphology trends with respect to the environment are calculated for each environmental variable, (1)–(4), in isolation from the others. For example, trends with increasing AOD and CAPE are shown without any attempt to understand the covariations in AOD and CAPE that might be dependently working to yield the observed trend. In the second part of the analysis, possible covariations between factors (1)–(4) as well as surface temperature and latitude are taken into account. Finally, some conclusions are offered.

## 2. Methods

This study makes use of two families of data. One set of data includes details of individual deep convective clouds, while the other data set contains information about the characteristics of the meteorological environment in which each cloud occurs. The environmental factors come from multiple sources, which are discussed at the end of this section. The approach to combining the cloud and environmental data is discussed in section 3.

### 2.1. Cloud Data

The information on clouds comes from a recently developed deep convective cloud database [*Igel et al*., 2014]. These data represent a very particular subset of CloudSat data. Only a brief description of the type of data included is presented.

CoudSat is a 94 GHz [*Stephens et al*., 2008] cloud-profiling radar in a Sun-synchronous orbit in the A-Train [*Stephens et al*., 2002]. It is sensitive to cloud droplets and raindrops and is attenuation corrected when appropriate. The cloud object data set is composed of observations from June 2006 to April 2011. The CloudSat data from which the database is constructed are first limited to the tropics (30°S to 30°N), to daytime, and to ocean only with sea surface temperatures between 298.5 K and 303.5 K. Attempts are then made to parse out mature deep convection in the following way. Cloudy cross-sectional regions are composed of contiguous pixels that exceed a variety of commonly used data thresholds in reflectivity and cloud mask ("cloudiness" and "certainty" thresholds, respectively). The resultant "cloud objects" are screened to ensure that they have a morphology that is consistent with mature, deep convection; the objects have a wide spreading anvil, a narrower region below this termed the "pedestal," and at least one convective "core" within this pedestal. Thus, the data set includes cross sections of deep convection that are similar in shape to the silhouette of vertically sliced mushrooms with sizes ranging from upright, individual, isolated cells to large, organized, potentially tilted cloud systems. From these cross sections, data are recorded for each cloud object as described below. Finally, certain data are checked for consistency, which ensures that the final cloud objects are high enough and have an anvil, for example. The result of these screening techniques is a data set composed of ~22,000 completely independent cloud objects, each with a variety of data that characterize that object. Extensive details on the thresholding and screening approach are included in *Igel et al*. [2014].

For the specific quantities that are frequently examined below, a brief description of the cloud morphological data is included here, while the details can be found in *Igel et al*. [2014]. Cloud top height (CTH) is a measure of the height above sea level of the highest pixel of the cloud object. Anvil width is a similarly simple measure of the distance between the two horizontally farthest apart cloudy pixels. The ice water path (IWP) measurement is calculated from the 2B-CWC-RVOD product [*Austin et al*., 2009] and is averaged over anvil pixels. Thus, the IWP measurement for any cloud object provides information about the average ice content across the whole anvil width. The anvil base temperature is the European Centre for Medium-Range Weather Forecasting (ECMWF) reanalysis temperature at the level at which the cloud object transitions in the vertical from pedestal-like to anvil-like characteristics. This level is objectively analyzed for each cloud object. Convective cores are identified using statistically significant minima and maxima pairs in horizontal cross sections of reflectivity in the cloud object pedestal [*Igel et al*., 2014].

It is important to consider the limitations imposed by the sampling geometry of the polar-orbiting CloudSat platform on these measurements. First, sampling is approximately meridional which could be important if clouds are preferentially oriented in space. Second, observations may not occur through the precise center of clouds. As a consequence of potentially being off-center, measurements discussed below are biased low on average since the maximum distance between any two points on a circle would occur along a diameter (i.e., would intersect the circle twice and pass through the center). Unfortunately, a precise quantification of the biases is difficult, but *Igel* [2014] suggests that they should not affect the conclusions drawn from the morphological measures discussed below. What we do not know at the current time is whether any of the environmental data to be considered affect clouds in such a way as to uniquely influence this bias. Determining the influence of environment on cloud orientation should be done in the future. While this cloud object data set comes with the limitations listed in this section, it nevertheless provides a pure and large data set from which numerous statistical conclusions can be drawn safely.

### 2.2. Environmental Data

The environmental data set utilized here makes use of a variety of observational and reanalysis platforms. AOD is taken from the Moderate Resolution Imaging Spectroradiometer (MODIS) [*Remer et al.*, 2005] on board the Aqua satellite. Collection 5.1 data are used at 10 km resolution. Because MODIS is aboard Aqua in the A-Train, an AOD observation occurs nearly simultaneously to a CloudSat observation. Only the highest quality assured ("QA") data are used. Highest QA retrievals are considered "very good" aerosol retrievals and are the most certain not to be contaminated by clouds. Their use often prevents the precise collocation of clouds and aerosol (see section 3).

CAPE values are calculated from profiles of temperature and humidity from the Atmospheric Infrared Sounder (AIRS) instrument on board the Aqua satellite [*Aumann et al.*, 2003]. The aim of AIRS data is to provide measurements within 1 K root-mean-square (RMS) and 20% RMS for temperature and relative humidity, respectively [*Susskind et al.*, 2006]. Data are taken from the AIRSX2RET product version 6. Depending on surface and tropopause characteristics, relevant data are recorded on ~12 standard vertical pressure levels spaced ~100 hPa apart. Due to the relatively coarse vertical resolution of the components contributing to the CAPE calculation, the calculation is performed in a simple way so as to converge for every profile. CAPE is calculated between the lowest available level of data (very often the surface layer) and the AIRS observed tropopause level. The equivalent potential temperature of the lowest layer is calculated, and then the vertically integrated deficiency of equivalent potential temperature at each level above the lowest up to the tropopause is converted to equivalent CAPE. Thus, this method represents an absolute upper limit to the real CAPE minus any accumulated convective inhibition. Other methods for calculating CAPE were attempted including iterative techniques. Ultimately, the simple CAPE calculation described above was chosen due to its successful convergence for every single column and because CAPE values tended to fall within consistent regimes regardless of the method used. The QA values of "good" and "Best" were used since a statistical approach is taken in this study. The statistical distribution of CAPE values is similar to that noted previously [*Ye et al.*, 1998; *Roff and Yano*, 2002].

Both shear and $\omega$500 are obtained from the European Centre for Medium-Range Weather Forecasting (ECMWF) ERA-I reanalysis product [*Simmons et al.*, 2007]. The shear value for any column is calculated as the magnitude of the vector difference between two layer vector-averaged winds. These two layers are the surface layer, 1000 hPa to 900 hPa, and the anvil outflow layer, 300 hPa to 100 hPa. The sensitivity of the results to the choice in layers used is discussed in section 4.3. The $\omega$500 is simply the vertical pressure velocity at 500 hPa.

## 3. Theoretical Framework

In this study, simple relationships between observed environmental characteristics and tropical, deep convective clouds are sought, with the overarching goal being to try to gain insight into the dependence of clouds on some aspects of their local environment. Both cloud and environmental quantities are assessed from instantaneous measures, which limit the strict attribution of cause. However, in order to infer such relationships between clouds and environmental perturbations, it is assumed that given sufficient cloud objects and enough observations of environmental quantities, that physically meaningful statistical relationships between clouds and environments can be created that offer insights into the

physical processes at work. Nevertheless, caution must be exercised in attempting to take the implications of these relationships too far [*Gryspeerdt et al*., 2014b]. Therefore, throughout what follows, appropriate caveats are provided alongside the proposed relationships.

Each environmental data set mentioned in section 2 is obtained at its highest possible resolution. MODIS AOD is acquired at level-2 resolution, 10 km. AIRS is obtained also at level-2 resolution, 45 km at nadir. ECMWF 0.75° (~80 km) data are used. These data are therefore of a spacing comparable to the size of convective pedestals O (10 km) and anvils O (100 km), which implies some horizontal resolution of spatial features in the near-convective environment outside of QA issues.

These environmental data need to be collocated with the cloud objects in some way. Given the central location of a cloud object from the database [*Igel et al*., 2014], the nearest available measurement (observation or reanalysis) is found. For gridded data from ECMWF, the collocation requires an assessment of time and of location. First, the nearest time is found; then the nearest pixel from that time slice is selected. For swath data from AIRS and MODIS, only spatial displacement is considered. All the swath data from the day on which the cloud object occurred are constructed onto a grid at the data's native resolution. The nearest pixel to the cloud object with quality-assured data is taken as the value for that cloud. Since AIRS and MODIS are both part of the A-train, the observation times of the cloud and environment are only seconds apart. The use of high-QA data means that the aerosol and potentially CAPE measurements and cloud are not precisely collocated since these may not be retrieved inside cloud and that the data may be representative of the cloud-adjacent environmental aerosol loading or CAPE as opposed to that contained directly within the specific cloud element.

Other studies have used interpolation to fill in missing data, to stitch together granules from observations, or to infer temporal evolution from gridded, time-sliced data [*Meskhidze et al*., 2009; *Gryspeerdt et al*., 2014a]. This approach is not taken here as it is not obvious for our purposes how to do this in a self-consistent way or even what kind of interpolation is appropriate in either time or space. The atmosphere could act in many different, potentially nonlinear ways. The approach taken here should not introduce many uncertainties or errors beyond those inherent in the retrievals or reanalysis.

Finally, it should be noted that the analysis is performed with respect to existing cloud objects. As in *Igel et al*. [2014], no attempt has been made to account for changes in the frequency of clouds with respect to different environmental conditions. Analyzing gridded frequencies, total sky coverage, or changes in lifetime would be impossible given the nature of this CloudSat data subset. Therefore, while simple trends are examined, caution is required in extending the results beyond what they actually show.

With the particular variables analyzed, CAPE, shear, AOD, and $\omega$500, we have tried to span an environmental parameter space across which theory suggests potential convective sensitivity. *Kaufman et al*. [2005] and *Jones and Christopher* [2010] spanned an even larger parameter space in their attempts to assess the sensitivity of low clouds to AOD. Their results might suggest that in some cases, the environmental data included here are only a subset of the potentially influential factors affecting cloud morphology. Nevertheless, the goal of this work is to further understand existing deep convection-environmental relationships.

## 4. Results and Discussion

The analysis that occurs below is statistical in nature. As a consequence, it is important to note that the physical mechanisms discussed are merely suggested. A statistical analysis such as is conducted here cannot explicitly elucidate physical processes. We strive to provide physical interpretation of our statistics, but we do not intend to overstate the level at which they are implied.

### 4.1. Single-Variable Trends

#### 4.1.1. CAPE

First, we examine the dependencies of deep convective morphology on CAPE. Figures 1a–1e show five different morphological trends as a function of CAPE. Similar figures are recreated for all of the environmental predictors, so it is worth describing the structure of Figure 1. Each panel shows a different aspect of cloud morphology plotted as a function of the observed environmental CAPE in two ways. The red line is a linear regression fit to the entire data scatter of each individual morphology-environment pair.

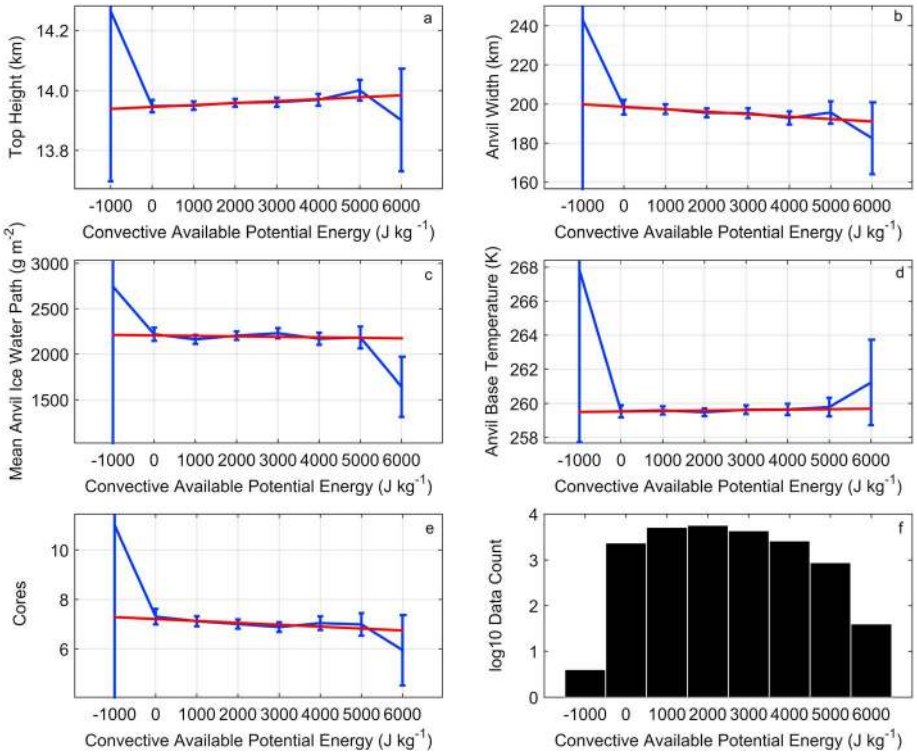


**Figure 1.** Each panel shows binned (1000 J kg$^{-1}$ width bins) means as a function of CAPE in blue. The 95% confidence interval for the mean of each bin is shown with the error bar. A linear regression to the unbinned data is shown in red. (a) Cloud top height. (b) Anvil width. (c) Mean anvil ice water path. (d) Anvil base temperature. (e) Number of convective cores. (f) The population of cloud objects that fall within each CAPE bin. Notice the logarithmic scale for Figure 1f.

The blue line shows mean morphological quantities for cloud data binned to the nearest thousand CAPE value. The 95% confidence intervals for the mean are calculated within each bin. These confidence intervals are statistical assessments of the exactness of the mean calculated for that bin and are plotted with error bars. Bin sizes are chosen so as to evenly span the range of data. Therefore, some bins only capture few clouds; the number of data points contributing to each bin is shown in Figure 1f. Again, specifically looking at Figure 1, the very first bin, −1000 J/kg, has only five contributing data, while the middle bins often have thousands. The −1000 J/kg CAPE bin and the highest AOD bin (Figure 2), which only has seven data pairs, are the least populated bins across all the various environmental predictor bins by a full order of magnitude, but these bins are included for completeness. The low CAPE bin has very large spread (Figures 1a–1e) and should probably be discounted, but the high AOD bin (Figure 2) often fits with trends and may be telling. The red line shows a linear regression fit and provides an unambiguous trend in the data, and the blue line is included to provide statistical information, namely, the potential bounds of the mean dictated by the population of objects. This line is included in lieu of showing the full scatterplot of data pairs. While the same data are used to compute both lines, the red regression fit is *not* computed directly from the blue, binned data.

Trends in cloud morphology are discussed and are arranged in Figure 1 from the cloud top downward. That is, they start with cloud top properties in Figure 1a and move downward to cloud core properties in Figure 1e. The trend in CTH with CAPE is shown in Figure 1a. Over the range of CAPE values in the data, CTH increases by approximately 100 m from ~14.35 km to ~14.45 km. This is likely due to the enhanced potential buoyancy of high CAPE atmospheres. Although an increase in CTH is observed, a larger trend may have been expected, as is discussed below in section 4.4. Anvil width decreases slightly from ~250 km to 230 km. Mean anvil ice water path remains approximately constant in the red, regression fit but decreases somewhat in the blue, binned data. Taken together, these results imply that anvils tend to get slightly higher and narrower with increasing CAPE but remain as dense. In Figure 1d, anvil base temperature is shown to be nearly constant. Figure 1e demonstrates that the trend in the number of identified convective cores within each convective

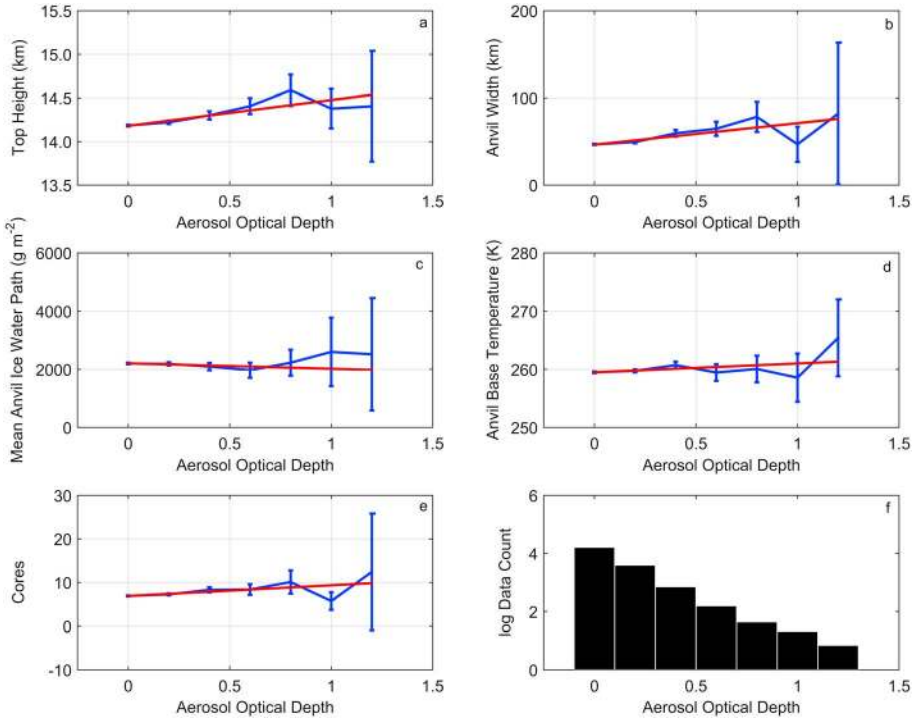


**Figure 2.** (a–f) Same as for Figure 1 except for AOD. The bin size is 0.25.

pedestal is slightly negative. A decreasing number of cores would seem to indicate that higher CAPE environments favor individual, isolated, single-core cloud objects over clusters or mesoscale convective systems, although this would be in contrast to that found in midlatitude storms [*Weisman and Klemp*, 1982] with the possible exception of supercells. The trends in the data as a function of CAPE are quite small, and only the trends in cloud top height and anvil width are statistically significant at better than the 0.05 level. Nevertheless, CAPE appears to exert a nontrivial influence on deep convective morphology.

#### 4.1.2. AOD

Cloud morphology trends with increasing aerosol concentration are analyzed using Figure 2 with an eye toward identifying evidence of aerosol invigoration. CTH increases substantially as AOD increases (Figure 2a). The red, regression fit increases by ~1 km over the range of AOD included here. Increasing CTH with increasing AOD is physically consistent with aerosol invigoration of deep convection [*Andreae et al*., 2004; *Khain et al*., 2005; *van den Heever et al*., 2006; *Koren et al*., 2010b; *Li et al*., 2011; *Storer and van den Heever*, 2013] and with past results from CloudSat [*Storer et al*., 2014]. Anvil width also tends to increase with increasing AOD. The combination of increasing CTH and anvil width with increasing AOD has been observed and discussed previously by *Koren et al*. [2010a] and *Yan et al*. [2014], both with different methods. *Fan et al*. [2013] postulated that since clouds in more polluted environments have smaller hydrometeors due to the increase in the number of particles able to serve as cloud condensation nuclei, anvils get wider as smaller hydrometeors can advect farther from their parent convection before precipitating. IWP exhibits an interesting behavior that is somewhat unique to AOD. The red, regression line decreases while the blue, binned line decreases before increasing substantially. These are actually somewhat independent behaviors since the AOD data are highly skewed toward low values over the tropical oceans. In this particular case, the binned data are more indicative of the behavior exhibited by the statistical scatter of the data at high AOD. So at high AOD, there seems to be an increase in mean IWP with higher AOD, while at lower AOD, it decreases. This dependence is remarkably similar to *Storer et al*. [2014] (their Figure 4d), who also made use of CloudSat data but not the cloud object data set used here; also, they used a very different aerosol data set. This result, along with the wider anvils, would imply more lofting of moisture in the clouds with highest AOD—a result consistent with aerosol-induced invigoration of updrafts and observed in *Storer and van den Heever* [2013]. That being said, Table 1 indicates that the trend in IWP is only significant at the 0.052 level. Anvil base temperature increases slightly, although the

**Table 1.** *P* Values for the Significance of the Linear Regression Trend for Each Environmental Variable and Morphology Measure Pair

| | Top Height | Anvil Width | Ice Water Path | Anvil Base Temperature | Number of Cores |
|---|---|---|---|---|---|
| CAPE | 0.019 | 0.016 | 0.38 | 0.62 | 0.051 |
| AOD | <0.01 | <0.01 | 0.052 | <0.01 | <0.01 |
| ω500 | <0.01 | <0.01 | 0.036 | <0.01 | <0.01 |
| Shear | <0.01 | <0.01 | <0.01 | <0.01 | <0.01 |

total trend is of a smaller magnitude than many of the confidence intervals. While a warming anvil base would seem inconsistent with invigoration, a potential explanation for this result is discussed in the next paragraph. Figure 2e shows that the number of convective cores per cloud object increases with increasing AOD. A similar result was suggested by *van den Heever et al*. [2011] in their analysis of aerosol impacts using a radiative convective equilibrium framework. This could be due to the strengthening of weaker updrafts in the presence of enhanced aerosol concentrations. Or this could be the result of some upscale process by which invigoration creates higher levels of organizational structure in the storm due to the wider or higher anvils (Figures 2a and 2b) or cold pool forcing. Over certain AOD ranges, we observe subtle nonlinear and nonmonotonic in behavior in various morphological measures. This kind of result has been hinted at across a wide range of aerosol-convective studies [e.g., *Li et al*., 2008; *Wang et al*., 2013; *Storer and van den Heever*, 2013].

Returning to the possible increase in anvil base temperature, the result seems counterintuitive as it might be expected that invigoration would result in colder (higher-altitude) anvil bases. We will argue that it is not. *Igel* [2014] postulated that the temperature at which anvil base occurs is a consequence of the maximum in depositional heating occurring at a defined temperature just below anvil base. The maximal heating occurs at this temperature and therefore so too does the maximum in convective updraft acceleration. Above this height, at the level of anvil base, the maximum convective vertical velocity occurs, which marks the level at which continuity requires horizontal divergence of air inside the pedestal to form an anvil. Aerosol could, in principle, affect the precise temperature at which the maximum in vapor deposition (and therefore the level of the anvil base) occurs by affecting microphysical process rates. If aerosol invigoration is occurring at high AOD, then more numerous, smaller hydrometeors of both a higher cumulative mass and cumulative volume are freezing heterogeneously within the updraft. These hydrometeors will continue to advect upward at the invigorated, higher vertical velocity. Deposition onto a distribution of particles that is higher in number and total mass occurs at an unambiguously higher rate [*Meyers et al*., 1997; *Pruppacher and Klett*, 2010]. Therefore, the maximum in deposition will occur at a lower altitude and higher temperature. Thus, not only could more latent heat of deposition be released due to a greater mass of hydrometeors advecting above the freezing level but also this latent heating could be occurring at a faster rate and at a lower height and higher temperature. We should stress that the increase in anvil base temperature occurs mostly at small AOD and is nonmonotonic in the blue, binned data. Therefore, these mechanisms and trends warrant future detailed investigation.

In summary, the AOD-morphology trends are broadly consistent with the idea of aerosol-induced convective invigoration. Storms get taller and wider and contain more anvil ice mass. Also noteworthy is the relatively high magnitude of some of the AOD trends in comparison to the weak trends seen in the CAPE discussion previously.

#### 4.1.3. The ω500

Morphological trends as a function of midlevel vertical velocity are shown in Figure 3. For consistency, trends are discussed with respect to increasing pressure velocity (increasing subsidence). The population of ω500 is clustered mostly between values of $-0.3\,\mathrm{hPa\,s^{-1}}$ and $0.2\,\mathrm{hPa\,s^{-1}}$ (Figure 3f) with a median value that is slightly negative at $-0.035\,\mathrm{hPa\,s^{-1}}$. This indicates a slight preference for cloud objects to occur in ascending regimes, a point that is discussed in detail in section 4.3. Interestingly, the results below often show a subtle difference between the red, regression fits and the blue, binned data at the extreme ends of the ω500 regime. At this time, we have no specific explanation for this behavior other than to suggest that individual clouds may respond nonlinearly outside of nearly neutral ω500 environments. The high percentage of cloud objects occurring in low-magnitude ω500 regimes would suggest a preference to occur at these near-neutral values.

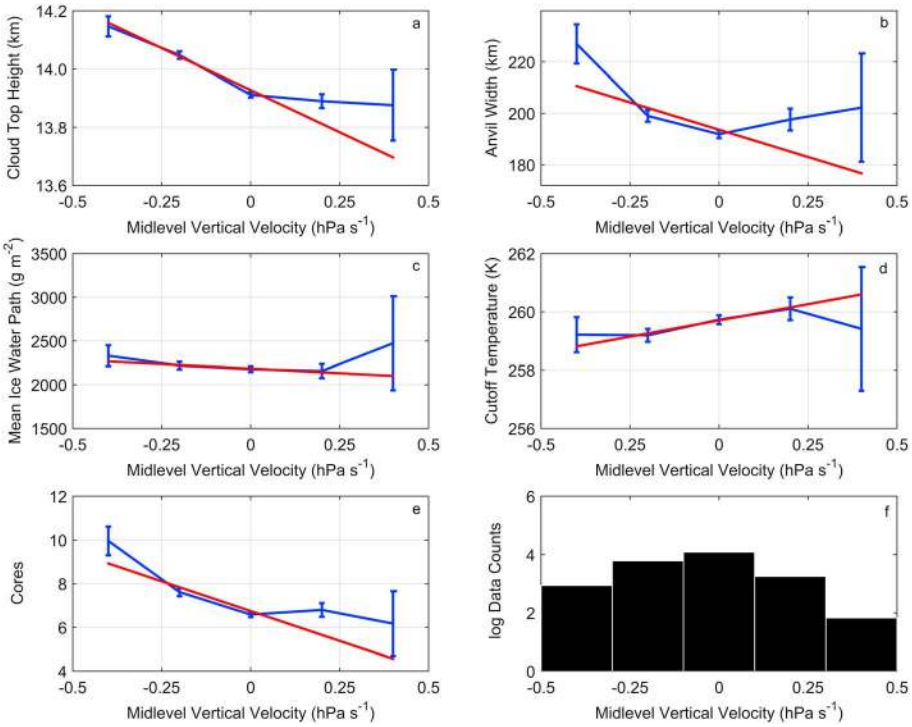


**Figure 3.** (a–f) Same as for Figure 1 except for ω500. The bin size is 0.20 hPa $s^{-1}$.

Figure 3a shows the trends in CTH as a function of midlevel pressure velocity. As the flow becomes increasingly subsident, CTH tends to decrease. The red, regression fit decreases more substantially than the blue, binned data, but both decrease by ~1 km over the range of ω500. This CTH trend makes physical sense because while environmental velocity becomes increasingly subsident, CTH vertical growth is stunted [*Bony et al.*, 2004]. Anvil width is one of the morphological measures for which the blue and red lines behave somewhat differently. The regression line decreases by ~30%, while the binned data decreases then increases. For the regression fit, it would seem that as the environment becomes more characterized by subsidence, anvils are becoming narrower. However, in the binned data, the global minimum in anvil width is actually at 0 hPa $s^{-1}$. This would mean that increasing the magnitude of ω500 would seem to favor wider anvils regardless of whether the air is rising or sinking. Certainly upward velocities could logically favor wider anvils by delaying hydrometeor fallout and through enhanced convective mass flux and detrainment, but how downward velocities do so is unclear. Anvil IWP is more logically consistent in its dependence on ω500; it generally decreases with increasing midlevel pressure velocity. Given that anvil base temperature rises slightly (Figure 3d) with increasing ω500, it would seem that this decrease in IWP can be attributed to shallower anvils arising from the decrease in CTH. The fall in anvil base temperature due to invigoration by ω500 (now with respect to decreasing ω500) stands in contrast to the rise associated with AOD. This result serves to emphasize the potential importance of the microphysical influence in the AOD results. The number of cores declines as subsidence increases (Figure 3e), which is indicative of the idea that rising air leads to a better chance of convection [*Bony et al.*, 1997, 2004; *Zelinka and Hartmann*, 2009] in the tropics.

#### 4.1.4. Shear

Figure 4 shows trends with respect to increasing troposphere-deep vertical shear of the horizontal wind. As stated above, the total shear is the magnitude of the vector difference of the mean winds between a surface layer (1000 hPa to 900 hPa) and the upper levels (300 hPa to 100 hPa). Of note is the general consistency between the binned data and the regression fits throughout Figure 4 and the narrow confidence intervals. As such, it is suggested that shear is a good monotonic predictor of cloud object morphology as has been found previously using other methods [*Rotunno et al.*, 1988; *LeMone et al.*, 1998; *Weisman and Rotunno*, 2004; *Coniglio et al.*, 2006].

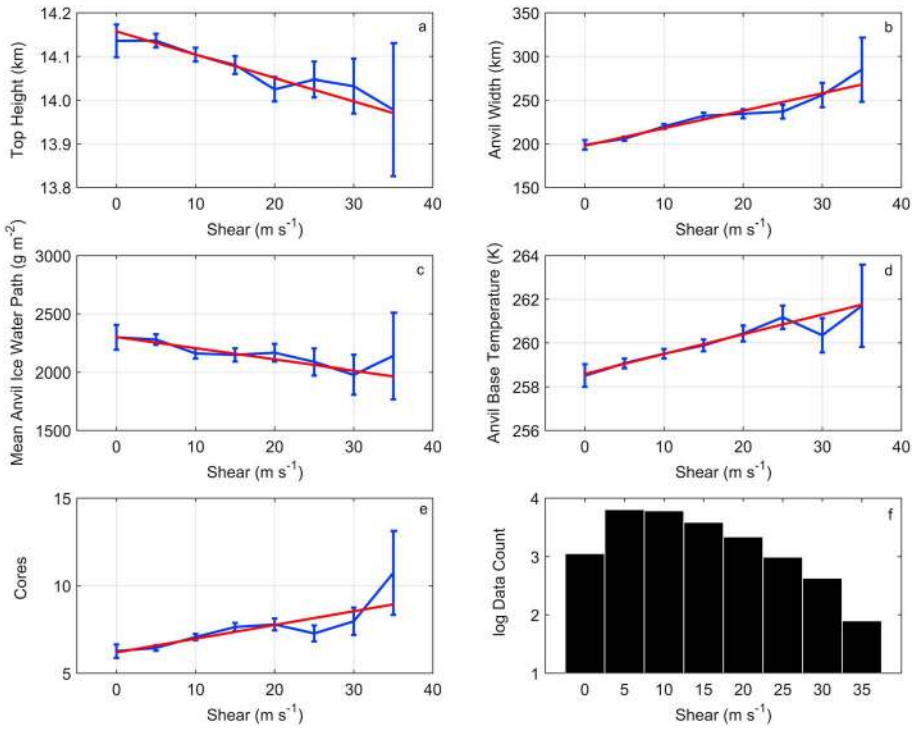


**Figure 4.** (a–f) Same as for Figure 1 except for shear. The bin size is 5 m $s^{-1}$.

Since all of the trends in morphology are consistent between the regression fits and the binned data, and since the trends form a cohesive picture of how the dynamics of clouds depend on shear, all of the trends are listed next and then discussed. As shear increases, CTH decreases, anvil width increases by close to a factor of 2, IWP decreases, the anvil base temperature increases, and the number of cores increases. As observed elsewhere [*Halverson et al*., 1999; *Saxen and Rutledge*, 2000; *Rickenbach et al*., 2008], anvils tend to become wider as they are blown further away from parent convection with increasing shear. The anvil thickness decreases for the same reason. Not only do their cloud top heights decrease, but it would also appear that their base heights decrease as well. This fact indicates that in this data set, shear tends to shrink storms vertically by enhancing horizontal widths at the expense of vertical development. The increase in core number is consistent with the observations that shear provides a means of storms organization in the tropics [*Saxen and Rutledge*, 2000; *Houze*, 2004].

### 4.2. Trend Attribution

In this section, the relative importance of each of the environmental variables discussed above is compared for each of the morphological trends presented. The goal is to determine which environmental factors contribute the most to cloud size and shape trends. Knowing which environmental characteristics are the most influential to cloud morphology could serve to help to construct future convective parameterizations.

The trend attribution is done with a series of multiple linear regressions. Environmental factors are used as "predictors" for morphological "dependents." All the predictors are normalized so as to occur over a range of (0,1), so that the regression coefficients can be compared easily. A higher regression coefficient therefore indicates a greater total influence by the respective predictor on the dependent variable. Despite this normalization, the statistical distributions of various predictors over the range (0,1) are often very different. For example, AOD is highly skewed toward zero, while ω500 is nearly normally distributed about 0.5. Finally, once regressions are computed, the coefficients are all normalized by the magnitude of the most significant predictor to ease interpretation. $R^2$ values for the regressions are often low given the spread in the dependent data, but residuals from the fit are often approximately Gaussian, so these values are not a cause for concern from a statistical point of view.

**Table 2.** The Linear Correlation Coefficient Among the Predictors

| | Latitude | SST | CAPE | ω500 | Shear | AOD |
|---|---|---|---|---|---|---|
| AOD | 0.046 | 0.016 | −0.023 | −0.031 | 0.053 | 1 |
| Shear | 0.006 | −0.20 | −0.012 | 0.090 | 1 | 0.053 |
| ω500 | 0.025 | −0.17 | −0.0052 | 1 | 0.090 | −0.031 |
| CAPE | −0.15 | 0.010 | 1 | −0.0052 | −0.012 | −0.023 |
| SST | −0.026 | 1 | 0.010 | −0.17 | −0.20 | 0.016 |
| Latitude | 1 | −0.026 | −0.15 | 0.025 | 0.006 | 0.046 |

Sea surface temperature (SST) and latitude are now added to the predictors already discussed. SST was used in *Igel et al*. [2014] as a dependent variable for convective morphology and is suggested by others [*Ramanathan and Collins*, 1991; *DeMott and Rutledge*, 1998a; *Lindzen et al*., 2001] as being influential to convection. Latitude is included as a proxy for a time-mean global scale flow regime. Not surprisingly, *Igel et al*. [2014] showed that the number of cloud objects exhibited a pattern in latitude similar to total cloud fraction as a function of latitude [*Sassen et al*., 2009].

In an effort to assess whether the environmental predictors are highly correlated (and therefore redundant), Table 2 lists the linear correlation coefficients among all of the environmental predictors associated with cloud objects. The highest-magnitude off-diagonal correlation is between SST and shear at −0.20, which is indicative of the fact that often there is locally more shear over lower SSTs. Next both SST and ω500, and latitude and CAPE, are negatively correlated with coefficients of −0.17 and −0.15, respectively. These results imply that upward vertical velocity increases over warmer SSTs [*Lau et al*., 1997] and that CAPE decreases poleward which may indicate a lowering tropopause height. Shear and ω500 are positively correlated at 0.090, which indicates higher shear in subsiding regions, and shear and AOD at 0.053, which is probably an indication of regional variability. All the other correlation coefficients are below 0.05. Most correlations are small, and while some physically based correlations are evident in the data, there is no reason to believe that any one of the environmental predictors is redundant. To confirm this, component analysis was conducted on the predictors. The analysis failed to successfully reduce the order of the data by more than one component despite the large number of cloud object samples. Nonetheless, the predictors do not appear to be linearly dependent on one another. So we may progress with some confidence in the knowledge that our predictors are mostly independent and well behaved.

Multiple linear regression results are shown in Figure 5. Each panel shows a bar plot of the regression coefficients for a different morphological dependent similar to the previous figures. Figure 5a displays the regression coefficients for CTH. SST is the leading predictor with ω500 and AOD approximately half as important as SST. SST is positively correlated with CTH, which indicates higher cloud tops and stronger convection with increasing SST as shown previously with this data set in *Igel et al*. [2014] and commonly. Anvil width correlations are shown in Figure 5b with four leading predictors indicated: ω500, SST, AOD, and shear. For IWP, the leading predictor is shear followed by AOD and SST. The leading predictor of anvil base temperature appears to be shear. The number of cores is most strongly correlated to ω500 strength. The statistical assessment of the values shown in Figure 5 indicates that all leading-order predictors are statistically significantly different than 0 at the 0.01 level (Table 3). Only for anvil width, IWP, and the number of cores is the root-mean-square error of the model residuals of the same order of magnitude as their mean value.

Taken together, the results of these multiple linear regressions imply that a certain subset of the environmental predictors is most influential to cloud morphology. Based on a qualitative assessment of Figure 5, shear appears to be the most significant predictor followed by SST. The ω500 is also frequently important. AOD is interesting in that it appears frequently in the leading predictor list above but always lags the leading predictor in magnitude for any individual morphological trend. What is also surprising is that CAPE is never a leading predictor (see section 4.4.1). Not only is the magnitude of the scaled regression coefficient often small for CAPE, but it also is sometimes 2 orders of magnitude smaller than the leading predictor.

Finally, all of these multiple linear regressions were recomputed with an additional predictor—one that would imply a constant value of the morphological dependent. That is, a new predictor of an arbitrary constant was included. This predictor does not represent any physical entity; it is merely mathematical and

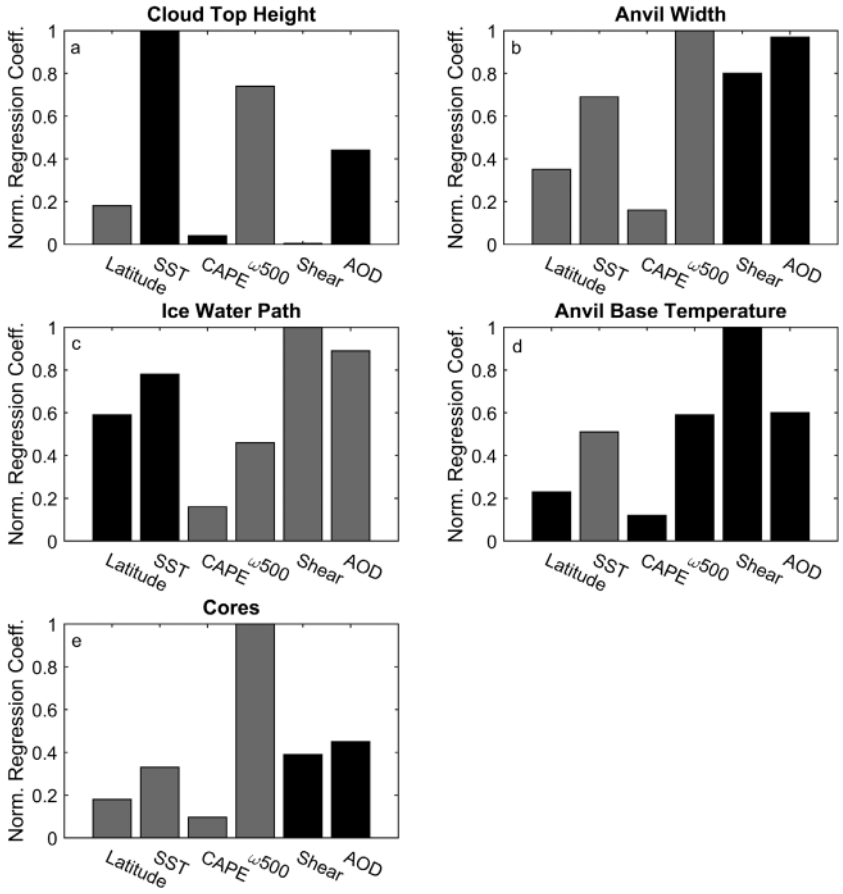


**Figure 5.** (a–e) Normalized multiple linear regression coefficients for each predictor (each bar) for the five morphological dependents (each panel) arranged as in Figure 1. The gray bars indicate negative values.

is included for statistical purposes. In all of the cases presented, this became the leading-order predictor. This result does not imply that cloud morphology is totally insensitive to the environment. But, it does imply a weak dependence on environment and a dependence of cloud morphology on cloud processes themselves. Lending further support to this suggestion, *Igel* [2014] found very strong correlations between sizes of various components of individual deep convective clouds. Although *Sherwood* [1999] cautions us explicitly against taking such statistical conclusions too far.

### 4.3. Data Control

In this section, we attempt to ensure that decisions made in appending the environmental data to the cloud objects do not unduly affect the analyzed trends. Toward that end, data are reanalyzed in various

**Table 3.** Predictor Significance and Normalized Error[a]

| | Top Height | Anvil Width | IWP | Anvil Base Temperature | Number of Cores |
|---|---|---|---|---|---|
| Latitude | <0.01 | <0.01 | 0.016 | 0.055 | <0.01 |
| SST | <0.01 | <0.01 | <0.01 | <0.01 | <0.01 |
| CAPE | 0.18 | <0.01 | 0.52 | 0.31 | 0.020 |
| ω500 | <0.01 | <0.01 | 0.20 | <0.01 | <0.01 |
| Shear | 0.88 | <0.01 | <0.01 | <0.01 | <0.01 |
| AOD | <0.01 | <0.01 | 0.052 | <0.01 | <0.01 |
| RMSE | 0.087 | 0.93 | 0.83 | 0.034 | 1.02 |

[a]For each morphological measure, the *P* value at which the multiple linear regression model coefficient for each predictor is significantly different from zero. The root-mean-square error of each multiple linear regression model normalized by the mean of that morphological measure.

**Table 4.** Control and Test Data[a]

| | Control Definition | Test Definition |
|---|---|---|
| AOD | 10 km resolution | 1° resolution and aerosol index |
| ω500 | Nearest-in-time | 0–6 h prior |
| Shear | Troposphere deep | Low level |
| SST | Local | Climatological anomaly |

[a]For each environmental variable, a list of the control definition of the data used throughout and a test definition of the data used in section 4.3.

ways in order to test some of the conclusions drawn above. It will be shown that the data used in section 4.1 constitute an appropriate set. Table 4 lists the original (control) and the new (test) data. Figure 6 shows the results of the multiple linear regressions using the test data.

First, an interesting comparison between slightly different AOD data sets was conducted. In general, as discussed above, the highest possible resolution environmental data were used in this study (see section 3). However, relationships obtained using different resolutions of AOD were also examined. Each cloud object has both a 10 km and 1° resolution AOD appended to it. The mean, median, standard deviation, and distribution shapes of these two quantities are remarkably similar. However, individual pairs of these values are often quite different. For example, a randomly chosen cloud object had a 10 km AOD of 0.24 and a 1° AOD of 0.33. Thus, the precise relationship between the cloud objects and AOD is slightly different. The mean and median distance between the observation center of AOD and the center of the cloud object are similar between the two sets of data, but the standard deviation and top 10% of distances are much greater for the 1° data. Thus, with no obvious cloud contamination at 10 km, or at least no more than exists at 1°, the 10 km data appear to be more representative of the clear-sky AOD local to the cloud. The 1° data did change some of the characteristics of the multiple linear regressions. It proved to be more influential to anvil width and core number than the 10 km data.

*Gryspeerdt et al*. [2014b] demonstrate that potentially unphysical conclusions can be drawn from correlating clouds and aerosol due to humidity swelling [*Twohy et al*., 2009], cloud contamination [*Kaufman et al*., 2005], and 3-D radiative effects [*Wen et al*., 2007]. However, the methodology employed here should help to

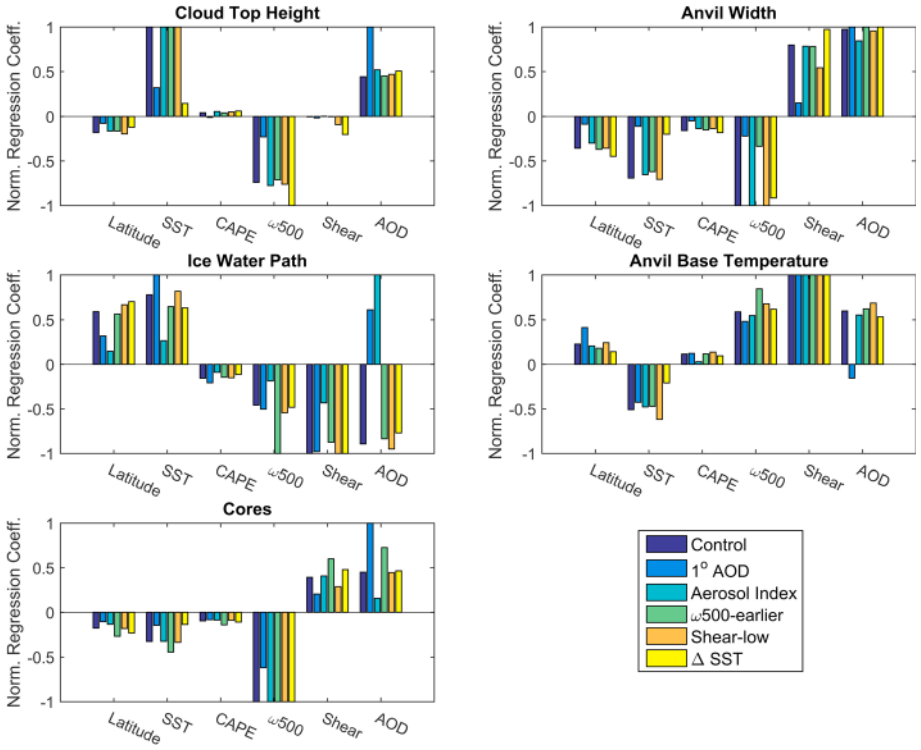


**Figure 6.** Similar to Figure 5 but utilizing the test data and with negative values below downward instead of gray. The color of the bar indicates the particular control data that have been replaced with test data. The dark blue bars show identical results to those in Figure 5. Only one data type is replaced at a time. For example, the yellow bars indicate the multiple linear regression coefficients for all variables in Figure 5 except that ω500 is replaced by ω500_earlier.

minimize such systematic errors that have been a problem previously, although it will not be able to eliminate correlated biases among aerosol measurements and dynamics [*Yuan et al.*, 2008]. Cloud objects rather than cloud fraction are utilized, and as such, all of the AOD retrievals used here should be similarly biased in the ways suggested. Over a large number of cloud objects, only the systematic biases from swelling, contamination, and radiative effects should be left. Since we then perform analyses with *trends* in AOD, and not *magnitudes*, the bias is precluded from influencing the conclusions.

Aerosol Index [*Nakajima et al.*, 2001] is sometimes used to characterize aerosol because it is thought to better correlate to cloud condensation nuclei number concentration than does AOD [*Lebsock et al.*, 2008; *Suzuki et al.*, 2013; *Wall et al.*, 2014]. The full analysis presented above was conducted again using Aerosol Index (AI) instead of AOD (Figure 6). The MODIS AI for 0.55 versus 0.86 is used. Trends and influence were mostly similar to AOD except for those in IWP. Curiously, the trend flipped sign and showed an increase in IWP with increasing AI. AI also became the leading predictor of IWP. It is not obvious why the use of AI would have such a different influence on IWP but little else when compared with AOD. Such a functional dependence of IWP does imply invigoration through measured increases in ice.

The remaining conceptual issue with $\omega$500 as an environmental variable is interpreting precisely what we are measuring. Because of the conditional sampling method used here where a cloud object is a necessary condition for $\omega$500 to be measured, understanding how much of the $\omega$500 field is due to what is traditionally thought of as $\omega$500, some kind of broad synoptic uplift, versus how much is due to the presence of cloud updraft is impossible. A reassignment of the data has been conducted in which $\omega$500 is defined to occur between 0 to 6 h prior to the observation of the cloud object. The data that were sampled originally between 0 and 3 h after the cloud object observation is replaced with data occurring 3 to 6 h prior to the cloud object observation. If cloud object lifetime is relatively short, this new "$\omega$500_earlier" measure will not be contaminated by the cloud-associated vertical motion. This simply serves as an illustrative check of the data quality as independence from cloud contamination is obviously not a realistic assumption. The mean arithmetic difference between the original $\omega$500 and the new $\omega$500_earlier indicates slightly more vertical motion in the original $\omega$500. This suggests that $\omega$500 is indeed slightly contaminated by the convection itself. Using this newly defined $\omega$500_earlier, all the trends in Figure 3 were then recalculated. In general, the trends became weaker, as would be expected for data characterizing physics that are less impactful to convection or data that are less influenced by the convection itself. Figure 6 shows that in aggregate, the $\omega$500_ealier data were no more influential when run through the multiple linear regressions. It may be concluded from this resampling that the original $\omega$500 is potentially influenced by the convection itself and that if this is the case, then trends attributed to $\omega$500 above are actually overestimates.

A conceptually different version of shear was also calculated. Shear_low is calculated as the magnitude of the vector difference between the 1000 hPa–900 hPa and 800 hPa–700 hPa layers. Often times, this low-level shear is assumed to be important for updraft morphology due to its ability to interact with the storm-produced cold pool [*Rotunno et al.*, 1988]. Shear_low was run through the same analysis as the deep-layer shear. The trends obtained were similar to those in Figure 4, although not as strong. The multiple linear regression coefficients were mostly slightly weaker. The only noteworthy change in the correlation coefficients was between shear_low and SST which decreased in magnitude to $-0.18$. Given its cumulative performance, the original shear formulation is better suited than shear_low as a predictor of the tropical deep convection morphology trends examined herein.

Finally, SST has been reassessed in terms of its departure from its 20 year (1991–2010) mean ($\Delta$SST) of its geographic location ($1^\circ \times 1^\circ$ bins). The mode of the histogram of cloud objects occurs at +1.5 K with a long tail toward positive anomalies and a short tail toward negative anomalies. The lowest $\Delta$SST of a cloud object occurs at just $-3.6$ K. Figure 6 indicates that $\Delta$SST is less influential than SST in every case (the orange bar is lower than the dark blue bar for the SST category). Only for IWP did it retain much predictive power. Another revealing assessment was also performed. In this case, trends were examined with respect to $\Delta$SST for a certain climatological-SST bin. For example, the anvil widths for cloud objects with a climatological SST of 300 K were regressed as a function of their $\Delta$SST. In these cases, $\Delta$SST was influential. Like the SST value used in section 4.2, this second $\Delta$SST casts morphology as a function of an absolute surface temperature—in this case as a departure from a specific value. The real conclusion to be

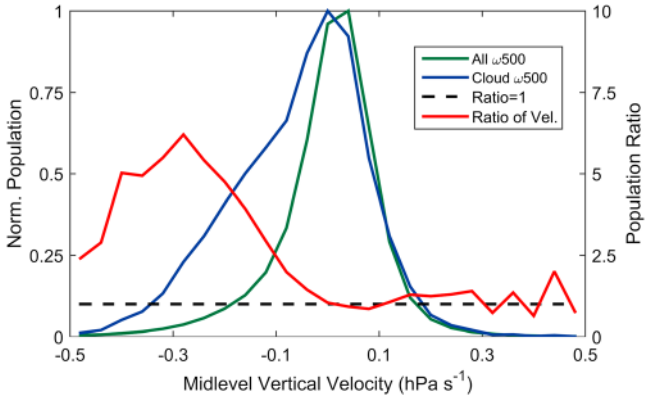


**Figure 7.** The blue and green lines illustrate the normalized population density of the cloud object-associated ω500 and the all-environment ω500, respectively. These values are read off the left axis. The red line is the ratio of blue to green and is read off the right axis. The black dashed line illustrates a constant ratio of 1.

drawn from the investigation of ΔSST is that a pure anomaly in SST does not appear to be particularly influential to cloud morphology; however absolute temperature does.

### 4.4. Potentially Surprising Insensitivities

The two results discussed that are potentially the most surprising are (1) the almost complete lack of sensitivity of cloud morphology to CAPE given that it frequently forms the basis of a number of parameterization schemes [*Arakawa*, 2004; *Yano and Plant*, 2012] and its demonstrated influence on midlatitude clouds [e.g., *Bluestein and Parker*, 1993; *Weisman*, 1993] and (2) that sensitivity to ω500 does not overwhelm the statistical signal coming from the other variables given past results [*Lau et al*., 1997]. These results are discussed next.

#### 4.4.1. CAPE

There are potentially two primary reasons cloud morphology is only weakly sensitive to CAPE. The first is that the retrieval and/or calculation of CAPE may be unrepresentative of environmental CAPE. AIRS data are relatively coarse and subject to contamination in high cloud fraction layers at low levels [*Yue et al*., 2013]. Consequently, it is possible that the CAPE measurement is often poorly representative of the real environmental CAPE. The second possible reason for CAPE's poor predictive skill is simply that in the tropics, deep convective clouds are physically insensitive to the precise magnitude of CAPE. This conclusion has been made before [e.g., *Mapes and Houze*, 1992]. The tropical atmosphere over open ocean tends to be characterized by constant, deep, and skinny CAPE [*Lucas et al*., 1994]. It has also been suggested that convection over the ocean is more prone to entrainment [*Lucas et al*., 1994], thus diluting the potential influence of CAPE. To date, it has not been demonstrated that a cloud needs to eliminate all of the CAPE in its environment; CAPE is simply a kind of upper bound on the potential kinetic energy a cloud can realize. In areas of weak lapse rates, total CAPE may be difficult for any storm to realize. Also, large CAPE values in the tropics would tend to result from anomalously dry upper levels. This condition, though, is mostly anathema to deep convection [*Brown and Zhang*, 1997]. Finally, the convective cloud itself might be depleting CAPE [*Masunaga*, 2012].

#### 4.4.2. Midlevel Vertical Velocity

That ω500 is not *the* leading predictor of convective morphology is likely to be especially surprising given past results to the contrary [*Lau et al*., 1997]. Again, there are two potential explanations for this result. The first is that precisely what constitutes the ω500 field in the ECMWF reanalysis is somewhat ill defined. In regions conditionally sampled to include deep convection, the field is a convolution of both background environmental vertical velocity and convective vertical velocity. This obscures its role. Second, it may simply be that while ω500 is a highly useful quantity in predicting where deep convection will occur, it is not *the* defining factor of what those clouds will look like. To confirm that cloud occurrence and morphology are different, Figure 7 shows the normalized (by maximum value, not integrated area) population densities (PDFs) of ω500 associated with cloud objects and all ω500 across the entire tropics. The PDF of cloud-object-ω500 is consistent with the first-order statistics listed above (section 4.1.3), and the tropics-wide-ω500 PDF exhibits expected behavior: a peak and skewness toward slightly positive values. Where these PDFs differ is at moderately negative values. The ratio of the two PDFs is also shown and exhibits a peak at $-0.3$ hPa s$^{-1}$. Therefore, cloud objects do occur preferentially in rising regimes, as would be expected. The implication of this figure is that the cloud object database does not exhibit an unrepresentative dependence on ω500 in cloud object occurrence. So it is consistent with past results and first principles, and yet ω500 still is not the sole dictate of morphology.

## 5. Summary

The sensitivity of mature tropical deep convective clouds to various environmental characteristics has been evaluated. Characteristics such as CAPE were shown to influence convective morphology only weakly, while others, including aerosol, shear, and SST, were shown to influence convection in significant and physically telling ways. The primary mechanisms elucidated through the various analysis methods above appear to include the following:

1. *convective invigoration by both aerosol and midlevel rising motion and to a lesser extent, CAPE*. Clouds in high AOD regimes are both deeper and wider. This is due to aerosol-induced deep convective invigoration. Aerosol invigoration also leads to anvil bases lowering in response to more intense updrafts due to microphysical processes. Midlevel rising motion results in similar changes in cloud morphology. It was suggested that this was the result of enhancements to convection from large-scale dynamics. Environments with higher CAPE also exhibit deeper and wider clouds, but the trends are small in comparison to those from aerosol and midlevel motion.
2. *storm organization and "shrinking" by troposphere-deep shear*. Cloud objects that exist in regions of larger tropospheric-deep shear are generally shorter than those in regions of weak shear. But, they are often wider with more convective cores, a result that complements contemporary theory.
3. *substantial control of morphology by sea surface temperature*. Multiple linear regressions reveal that sea surface temperature is among the important influences to convective morphology. This result strengthens the results of a previous study [*Igel et al*., 2014].

As was deemed appropriate, the sensitivity of results to choices made in defining the environment was tested. It was found that the data used throughout formed a reasonable basis set. The weak sensitivity to CAPE of morphology was attributed to a lack of physical control pathways. Midlevel vertical velocity was shown to be influential but not overwhelmingly so.

It is important to remember two things about the results presented. First, we cannot possibly hope to probe all of the possible influences to highly dynamic, turbulent entities such as deep convective clouds. Therefore, what we have striven to show are often small trends in highly variable data. Second, our results are purely statistical. As such, we can only indirectly imply physical mechanisms responsible for such results. Care has been taken to do this in as meaningful a way as possible.

The goal in performing this analysis was to assess the sensitivity of oceanic, tropical, deep convective cloud morphology to the local meteorological environment. While no specific recommendations have been made concerning convective parameterizations, the implication of these CloudSat-based results is that cloud morphology probably can be parameterized based on simple diagnostics of the environmental characteristics. Certainly, CAPE is already used extensively, and aerosol loading is beginning to be utilized [e.g., *Abdul-Razzak and Ghan*, 2000]. Any parameterization that seeks to be more inclusive of environmental parameters will be challenged to determine the right set of predictors. The results above would suggest that aerosol, midlevel velocity, deep-layer shear, and SST would be a useful basis set from which to continue development.

**Acknowledgments**
The authors would like to thank the three anonymous reviewers for their helpful suggestions which resulted in a more precise discussion. This work was supported by NASA CloudSat grant 5–319160. This work was also supported by NASA Headquarters under the NASA Earth and Space Science Fellowship Program grant NNX 13AN66H.
The authors would like to thank J. zumBrunnen of the CSU Statistical Laboratory for the helpful discussion on the analysis and A. Igel for the useful suggestions. Data can be obtained by contacting M. Igel (migel@rsmas.miami.edu).

## References

Abdul-Razzak, H., and S. Ghan (2000), A parameterization of aerosol activation: 2. Multiple aerosol types, *J. Geophys. Res.*, *105*(D5), 6837–6844, doi:10.1029/1999JD901161.
Andreae, M. O. (2009), Correlation between cloud condensation nuclei concentration and aerosol optical thickness in remote and polluted regions, *Atmos. Chem. Phys.*, *9*, 543–556.
Andreae, M., D. Rosenfeld, P. Artaxo, A. Costa, G. Frank, K. Longo, and M. Silva-Dias (2004), Smoking rain clouds over the Amazon, *Science*, *303*, 1337–1342.
Arakawa, A. (2004), The cumulus parameterization problem: Past, present, and future, *J. Clim.*, *17*(13), 2493–2525.
Aumann, H. H., et al. (2003), AIRS/AMSU/HSB on the Aqua mission: Design, science objectives, data products, and processing systems, *IEEE Trans. Geosci. Remote Sens.*, *41*, 253–264.
Austin, R. T., A. J. Heymsfield, and G. L. Stephens (2009), Retrieval of ice cloud microphysical parameters using the CloudSat millimeter-wave radar and temperature, *J. Geophys. Res.*, *114*, D00A23, doi:10.1029/2008JD010049.
Barnes, G. M., and K. Sieckman (1984), The environment of fast- and slow-moving tropical mesoscale convective cloud lines, *Mon. Weather Rev.*, *112*, 1782–1794.
Bluestein, H. B., and S. S. Parker (1993), Modes of isolated, severe convective storm formation along the dryline, *Mon. Weather Rev.*, *121*, 1354–1372.
Bony, S., K.-M. Lau, and Y. C. Sud (1997), Sea surface temperature and large-scale circulation influences on tropical greenhouse effect and cloud radiative forcing, *J. Clim.*, *10*(8), 2055–2077, doi:10.1175/1520-0442(1997)010<2055:SSTALS>2.0.CO;2.

Bony, S., J.-L. Dufresne, H. Le Treut, J.-J. Morcrette, and C. Senior (2004), On dynamic and thermodynamic components of cloud changes, *Clim. Dyn.*, *22*(2–3), 71–86, doi:10.1007/s00382-003-0369-6.
Brown, R. G., and C. D. Zhang (1997), Variability of midtropospheric moisture and its effect on cloud-top height distribution during TOGA COARE, *J. Atmos. Sci.*, *54*(23), 2760–2774.
Cetrone, J., and R. A. Houze (2006), Characteristics of tropical convection over the ocean near Kwajalein, *Mon. Weather Rev.*, *134*(3), 834–853, doi:10.1175/MWR3075.1.
Coniglio, M. C., D. J. Stensrud, and L. J. Wicker (2006), Effects of upper-level shear on the structure and maintenance of strong quasi-linear mesoscale convective systems, *J. Atmos. Sci.*, *63*, 1231–1252.
Del Genio, A. D., and W. Kovari (2002), Climatic properties of tropical precipitating convection under varying environmental conditions, *J. Clim.*, *15*(18), 2597–2615.
DeMott, C. A., and S. A. Rutledge (1998a), The vertical structure of TOGA COARE convection. Part I: Radar echo distributions, *J. Atmos. Sci.*, *55*, 2730–2747.
DeMott, C. A., and S. A. Rutledge (1998b), The vertical structure of TOGA COARE convection. Part II: Modulating influences and implications for diabatic heating, *J. Atmos. Sci.*, *55*, 2748–2762.
Fan, J., T. Yuan, J. M. Comstock, S. Ghan, A. Khain, L. R. Leung, Z. Li, V. J. Martins, and M. Ovchinnikov (2009), Dominant role by vertical wind shear in regulating aerosol effects on deep convective clouds, *J. Geophys. Res.*, *114*, D22206, doi:10.1029/2009JD012352.
Fan, J., L. R. Leung, D. Rosenfeld, Q. Chen, Z. Li, J. Zhang, and H. Yan (2013), Microphysical effects determine macrophysical response for aerosol impacts on deep convective clouds, *Proc. Natl. Acad. Sci. U.S.A.*, *110*(48), E4581–E4590, doi:10.1073/pnas.1316830110.
Gryspeerdt, E., P. Stier, and D. G. Partridge (2014a), Links between satellite retrieved aerosol and precipitation, *Atmos. Chem. Phys. Discuss.*, *14*(5), 6821–6861, doi:10.5194/acpd-14-6821-2014.
Gryspeerdt, E., P. Stier, and D. G. Partridge (2014b), Satellite observations of cloud regime development: The role of aerosol processes, *Atmos. Chem. Phys.*, *14*(3), 1141–1158, doi:10.5194/acp-14-1141-2014.
Halverson, J. B., B. S. Ferrier, T. M. Rickenbach, J. Simpson, and W. Tao (1999), An ensemble of convective systems on 11 February 1993 during TOGA COARE: Morphology, rainfall characteristics, and anvil cloud interactions, *Mon. Weather Rev.*, *127*, 1208–1228.
Hildebrand, P. H. (1998), Shear-parallel moist convection over the tropical ocean: A case study from the 18 February 1993 TOGA COARE, *Mon. Weather Rev.*, *126*, 1952–1976.
Houze, R. A. (2004), Mesoscale convective systems, *Rev. Geophys.*, *42*, RG4003, doi:10.1029/2004RG000150.
Houze Jr., R. A., and C.-P. Cheng (1977), Radar characteristics of tropical convection observed during GATE: Mean properties and trends over the summer season, *Mon. Weather Rev.*, *105*, 964–980.
Igel, M. R. (2014), Tropical deep convective cloud morphology, PhD dissertation, 181, Colorado State Univ., Fort Collins.
Igel, M. R., A. J. Drager, and S. C. van den Heever (2014), A CloudSat cloud object partitioning technique and assessment and integration of deep convective anvil sensitivities to sea surface temperature, *J. Geophys. Res. Atmos.*, *119*, 10,515–10,535, doi:10.1002/2014JD021717.
Johnson, R. H., T. M. Rickenbach, S. A. Rutledge, P. E. Ciesielski, and W. H. Schubert (1999), Trimodal characteristics of tropical convection, *J. Clim.*, *12*, 2397–2418.
Johnson, R. H., S. A. Aves, P. E. Ciesielski, and T. D. Keenan (2005), Organization of oceanic convection during the onset of the 1998 East Asian summer monsoon, *Mon. Weather Rev.*, *133*, 131–148.
Jones, T. A., and S. A. Christopher (2010), Statistical properties of aerosol-cloud-precipitation interactions in South America, *Atmos. Chem. Phys.*, *10*, 2287–2305.
Kaufman, Y. J., I. Koren, L. A. Remer, D. Rosenfeld, and Y. Rudich (2005), The effect of smoke, dust, and pollution aerosol on shallow cloud development over the Atlantic Ocean, *Proc. Natl. Acad. Sci. U.S.A.*, *102*(32), 11,207–11,212, doi:10.1073/pnas.0505191102.
Khain, A., D. Rosenfeld, and A. Pokrovsky (2005), Aerosol impact on the dynamics and microphysics of deep convective clouds, *Q. J. R. Meteorol. Soc.*, *131*, 2639–2664.
Koren, I., G. Feingold, and L. A. Remer (2010a), The invigoration of deep convective clouds over the Atlantic: Aerosol effect, meteorology, or retrieval artifact?, *Atmos. Chem. Phys.*, *10*, 8855–8872, doi:10.5194/acp-10-8855-2010.
Koren, I., L. A. Remer, O. Altaratz, J. V. Martins, and A. Davidi (2010b), Aerosol-induced changes of convective cloud anvils produce strong climate warming, *Atmos. Chem. Phys.*, *10*(10), 5001–5010, doi:10.5194/acp-10-5001-2010.
Kumar, V. V., A. Protat, C. Jakob, and P. T. May (2014), On the atmospheric regulation of the growth of moderate to deep cumulonimbus in a tropical environment, *J. Atmos. Sci.*, *71*(3), 1105–1120, doi:10.1175/JAS-D-13-0231.1.
Lau, K.-M., T.-U. Wu, and S. Bony (1997), The role of large-scale atmospheric circulation in the relationship between tropical convection and sea surface temperature, *J. Clim.*, *10*, 381–392.
Lebsock, M. D., G. L. Stephens, and C. Kummerow (2008), Multisensor satellite observations of aerosol effects on warm clouds, *J. Geophys. Res.*, *113*, D15205, doi:10.1029/2008JD009876.
LeMone, M. A., E. J. Zipser, and S. B. Trier (1998), The role of environmental shear and thermodynamic conditions in determining the structure and evolution of mesoscale convective systems during TOGA COARE, *J. Atmos. Sci.*, *55*(23), 3493–3518, doi:10.1175/1520-0469(1998)055<3493:TROESA>2.0.CO;2.
Li, W., and C. Schumacher (2011), Thick anvils as viewed by the TRMM precipitation radar, *J. Clim.*, *24*, 1718–1735.
Li, G., Y. Wang, and R. Zhang (2008), Implementation of a two-moment bulk microphysics scheme to the WRF model to investigage aerosol-cloud interaction, *J. Geophys. Res.*, *113*, D15211, doi:10.1029/2007JD009361.
Li, Z., F. Niu, J. Fan, Y. Liu, D. Rosenfeld, and Y. Ding (2011), Long-term impacts of aerosols on the vertical development of clouds and precipitation, *Nat. Geosci.*, *4*, 888–894, doi:10.1038/NGEO1313.
Lindzen, R. S., M. Chou, and A. Y. Hou (2001), Does the Earth have an adaptive infrared iris?, *Bull. Am. Meteorol. Soc.*, *82*(3), 417–432.
Liu, C., and E. J. Zipser (2013), Regional variation of morphology of the organized convection in the tropics and subtropics, Part I: Regional variation, *J. Geophys. Res. Atmos.*, *118*, 453–466, doi:10.1029/2012JD018409.
Lucas, C., E. J. Zipser, and M. A. LeMone (1994), Vertical velocity in oceanic convection off tropical Australia, *J. Atmos. Sci.*, *51*(21), 3183–3193.
Mapes, B., and R. A. Houze (1992), An integrated view of the 1987 Australian monsoon and its mesoscale convective systems. I: Horizontal structure, *Q. J. R. Meteorol. Soc.*, *118*, 927–963.
Masunaga, H. (2012), A satellite study of the atmospheric forcing and response to moist convection over tropical and subtropical oceans, *J. Atmos. Sci.*, *69*(1), 150–167, doi:10.1175/JAS-D-11-016.1.
Masunaga, H., T. S. L'Ecuyer, and C. D. Kummerow (2005), Variability in the Characteristics of Precipitation Systems in the Tropical Pacific. Part I: Spatial Structure, *J. Clim.*, *18*, 823–840.
Meskhidze, N., L. A. Remer, S. Platnick, R. Negron, A. M. Lichtenberger, and A. R. Aiyyer (2009), and Physics Exploring the differences in cloud properties observed by the Terra and Aqua MODIS sensors, *Atmos. Chem. Phys.*, *9*, 3461–3475.

Meyers, M. P., R. L. Walko, J. Y. Harrington, and R. Cotton (1997), New RAMS microphysics parameterization. Part II: The two-moment scheme, *Atmos. Res.*, *45*, 3–39.
Nakajima, T., A. Higurashi, K. Kawamoto, and J. E. Penner (2001), A possible correlation between satellite-derived cloud and aerosol microphysical parameters, *Geophys. Res. Lett.*, *28*(7), 1171–1174, doi:10.1029/2000GL012186.
Nesbitt, S. W., and E. J. Zipser (2003), The diurnal cycle of rainfall and convective intensity according to three years of TRMM measurements, *J. Clim.*, *16*(10), 1456–1475.
Nesbitt, S. W., E. J. Zipser, and D. J. Cecil (2000), A census of precipitation features in the tropics using TRMM: Radar, ice scattering, and lightning observations, *J. Clim.*, *13*(23), 4087–4106.
Nesbitt, S. W., R. Cifelli, and S. A. Rutledge (2006), Storm morphology and rainfall characteristics of TRMM precipitation features, *Mon. Weather Rev.*, *134*(10), 2702–2721.
Niu, F., and Z. Li (2012), Systematic variations of cloud top temperature and precipitation rate with aerosols over the global tropics, *Atmos. Chem. Phys.*, *12*, 8491–8498, doi:10.5194/acp-12-8491-2012.
Peters, K., C. Jakob, L. Davies, B. Khouider, and A. J. Majda (2013), Stochastic behavior of tropical convection in observations and a multicloud model, *J. Atmos. Sci.*, *70*(11), 3556–3575, doi:10.1175/JAS-D-13-031.1.
Pruppacher, H. R., and J. D. Klett (2010), *Microphysics of Clouds and Precipitation*, 2nd ed., pp. 954, Springer, New York.
Ramanathan, V., and W. Collins (1991), Thermodynamic regulation of ocean warming by cirrus clouds deduced from observations of the 1987 El Niño, *Nature*, *351*, 27–32.
Remer, L. A., et al. (2005), The MODIS aerosol algorithm, products, and validation, *J. Atmos. Sci.*, *62*(4), 947–973, doi:10.1175/JAS3385.1.
Rickenbach, T., P. Kucera, M. Gentry, L. Carey, A. Lare, R.-F. Lin, B. Demoz, and D. O. Starr (2008), The relationship between anvil clouds and convective cells: A case study in South Florida during CRYSTAL-FACE, *Mon. Weather Rev.*, *136*(10), 3917–3932, doi:10.1175/2008MWR2441.1.
Riley, E. M., B. E. Mapes, and S. N. Tulich (2011), Clouds associated with the Madden–Julian oscillation: A new perspective from CloudSat, *J. Atmos. Sci.*, *68*(12), 3032–3051, doi:10.1175/JAS-D-11-030.1.
Roff, G. L., and J.-I. Yano (2002), Tropical convective variability in the CAPE phase space, *Q. J. R. Meteorol. Soc.*, *128*(585), 2317–2333, doi:10.1256/qj.01.138.
Rosenfeld, D., U. Lohmann, G. Raga, C. O'Dowd, M. Kulmala, S. Fuzzi, A. Reissell, and M. Andreae (2008), Flood or drought: How do aerosols affect precipitation?, *Science*, *321*, 1309–1313, doi:10.1126/science.1160606.
Rotunno, R., J. B. Klemp, and M. L. Weisman (1988), A theory for strong, long-lived squall lines, *J. Atmos. Sci.*, *45*(3), 463–485.
Sassen, K., Z. Wang, and D. Liu (2009), Cirrus clouds and deep convection in the tropics: Insights from CALIPSO and CloudSat, *J. Geophys. Res.*, *114*, D00H06, doi:10.1029/2009JD011916.
Saxen, T. R., and S. A. Rutledge (2000), Surface rainfall–cold cloud fractional coverage relationship in TOGA COARE: A function of vertical wind shear, *Monthly*, *128*, 407–415.
Schneider, T., P. A. O'Gorman, and X. J. Levine (2010), Water vapor and the dynamics of climate changes, *Rev. Geophys.*, *48*, RG3001, doi:10.1029/2009RG000302.
Sherwood, S. C. (1999), Convective precursors and predictability in the tropical western Pacific, *Mon. Weather Rev.*, *127*, 2977–2991.
Simmons, A., S. Uppala, D. Dee, and S. Kobayashi (2007), The ERA Interim reanalysis, *ECMWF Newsl.*, *110*, 25–35.
Stephens, G. L. (2005), Cloud feedbacks in the climate system: A critical review, *J. Clim.*, *18*(2), 237–273.
Stephens, G. L., et al. (2002), The Cloudsat mission and the A-Train, *Bull. Am. Meteorol. Soc.*, *83*(12), 1771–1790, doi:10.1175/BAMS-83-12-1771.
Stephens, G. L., et al. (2008), CloudSat mission: Performance and early science after the first year of operation, *J. Geophys. Res.*, *113*, D00A18, doi:10.1029/2008JD009982.
Storer, R. L., and S. C. van den Heever (2013), Microphysical processes evident in aerosol forcing of tropical deep convective clouds, *J. Atmos. Sci.*, *70*, 430–446.
Storer, R. L., S. C. Van Den Heever, and T. S. L. Ecuyer (2014), Observations of aerosol-induced convective invigoration in the tropical East Atlantic, *J. Geophys. Res. Atmos.*, *119*, 3963–3975, doi:10.1002/2013JD020272.
Susskind, J., C. Barnet, J. Blaisdell, L. Iredell, F. Keita, L. Kouvaris, G. Molnar, and M. Chahine (2006), Accuracy of geophysical parameters derived from Atmospheric Infrared Sounder/Advanced Microwave Sounding Unit as a function of fractional cloud cover, *J. Geophys. Res.*, *111*, D09S17, doi:10.1029/2005JD006272.
Suzuki, K., G. L. Stephens, and M. D. Lebsock (2013), Aerosol effect on the warm rain formation process: Satellite observations and modeling, *J. Geophys. Res. Atmos.*, *118*, 170–184, doi:10.1002/jgrd.50043.
Tao, W., J. Chen, Z. Li, C. Wang, and C. Zhang (2012), Impact of aerosols on convective clouds and precipitation, *Rev. Geophys.*, *50*, RG2001, doi:10.1029/2011RG000369.
Twohy, C. H., J. A. Coakley, and W. R. Tahnk (2009), Effect of changes in relative humidity on aerosol scattering near clouds, *J. Geophys. Res.*, *114*, D05205, doi:10.1029/2008JD010991.
van den Heever, S. C., and W. R. Cotton (2007), Urban aerosol impacts on downwind convective storms, *J. Appl. Meteorol. Climatol.*, *46*, 828–850.
van den Heever, S. C., G. G. Carrio, W. R. Cotton, P. J. DeMott, and A. J. Prenni (2006), Impacts of nucleating aerosol on Florida storms. Part I: Mesoscale simulations, *J. Atmos. Sci.*, *63*, 1752–1775.
van den Heever, S. C., G. L. Stephens, and N. B. Wood (2011), Aerosol indirect effects on tropical convection characteristics under conditions of radiative-convective equilibrium, *J. Atmos. Sci.*, *68*, 699–718.
Wall, C., E. Zipser, and C. Liu (2014), An investigation of the aerosol indirect effect on convective intensity using satellite observations, *J. Atmos. Sci.*, *71*(1), 430–447, doi:10.1175/JAS-D-13-0158.1.
Wang, Y., A. Khalizov, M. Levy, and R. Zhang (2013), New directions: Light absorbing aerosols and their atmospheric impacts, *Atmos. Environ.*, *81*, 713–75, doi:10.1016/j.atmosenv.2013.09.034.
Weisman, M. L. (1993), The genesis of severe, long-lived bow echoes, *J. Atmos. Sci.*, *50*, 645–670.
Weisman, M. L., and J. B. Klemp (1982), The dependence of numerically simulated convective storms on vertical wind shear and buoyancy, *Mon. Weather Rev.*, *110*, 504–520.
Weisman, M. L., and R. Rotunno (2004), "A theory for strong long-lived squall lines" revisited, *J. Atmos. Sci.*, *61*(4), 361–382, doi:10.1175/1520-0469(2004)061<0361:ATFSLS>2.0.CO;2.
Wen, G., A. Marshak, R. Cahalan, L. Remer, and R. Kleidman (2007), 3-D aerosol-cloud radiative interaction observed in collocated MODIS and ASTER images of cumulus cloud fields, *J. Geophys. Res.*, *112*, D13204, doi:10.1029/2006JD008267.
Yan, H., Z. Li, J. Hunag, M. Cribb, and J. Liu (2014), Long-term aerosol-mediated changes in cloud radiative forcing of deep clouds at the top and bottom of the atmosphere over the Southern Great Plains, *Atmos. Chem. Phys.*, *14*, 7113–7124, doi:10.5194/acp-14-7113-2014.

Yano, J., and R. S. Plant (2012), Convective quasi-equilibrium, *Rev. Geophys.*, *50*, 1–30, doi:10.1029/2011RG000378.
Ye, B., A. D. Del Genio, and K. K.-W. Lo (1998), CAPE variations in the current climate and in a climate change, *J. Clim.*, *11*, 1997–2015.
Yuan, T., Z. Li, R. Zhang, and J. Fan (2008), Increase of cloud droplet size with aeorosol optical depth: An observation and modeling study, *J. Geophys. Res.*, *113*, D04201, doi:10.1029/2007JD008632.
Yue, Q., E. J. Fetzer, B. H. Kahn, S. Wong, G. Manipon, A. Guillaume, and B. Wilson (2013), Cloud-state-dependent sampling in AIRS observations based on CloudSat cloud classification, *J. Clim.*, *26*(21), 8357–8377, doi:10.1175/JCLI-D-13-00065.1.
Zelinka, M. D., and D. L. Hartmann (2009), Response of humidity and clouds to tropical deep convection, *J. Clim.*, *22*(9), 2389–2404, doi:10.1175/2008JCLI2452.1.